analytical chemistry

Article

Cite This: Anal. Chem. 2018, 90, 10179−10186

pubs.acs.org/ac

Label-Free Infrared Spectroscopy and Imaging of Single Phospholipid Bilayers with Nanoscale Resolution

Adrian Cernescu,[†] Michał Szuwarzyński,[‡] Urszula Kwolek,[§] Paweł Wydro,[§] Mariusz Kepczynski,[§] Szczepan Zapotoczny,[§] Maria Nowakowska,[§] and Luca Quaroni*[,§]

[†]Neaspec GmbH, Bunsenstrasse 5, 82152, Martinsried, Germany

[‡]Academic Centre for Materials and Nanotechnology, AGH University of Science and Technology, al. A. Mickiewicza 30, 30-059, Kraków, Poland

[§]Faculty of Chemistry, Jagiellonian University, ul. Gronostajowa 2, 30-387, Kraków, Poland

Supporting Information

ABSTRACT: Mid-infrared absorption spectroscopy has been used extensively to study the molecular properties of cell membranes and model systems. Most of these studies have been carried out on macroscopic samples or on samples a few micrometers in size, due to constraints on sensitivity and spatial resolution with conventional instruments that rely on far-field optics. Properties of membranes on the scale of nanometers, such as in-plane heterogeneity, have to date eluded investigation by this technique. In the present work, we demonstrate the capability to study single bilayers of phospholipids with near-field mid-infrared spectroscopy and imaging and achieve a spatial resolution of at least 40 nm, corresponding to a sample size of the order of a thousand molecules. The quality of the data and the observed spectral features are consistent with those reported from measurements of macroscopic samples and allow detailed analysis of molecular properties, including orientation and ordering of phospholipids. The work opens the way to the nanoscale characterization of the biological membranes for which phospholipid bilayers serve as a model.

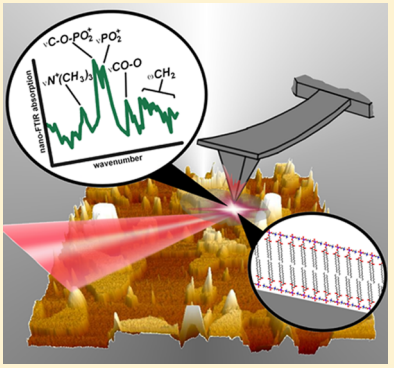

Membranes are defining structures of cells. Their role, however, extends beyond basic compartmentalization and includes overall organization of proteins in space and time, energy storage, control of trafficking and homeostatic regulation, intracellular and intercellular signal transduction, recognition, and adhesion. Despite intense interest, many issues related to the structure and function of membranes are still unaddressed or there is no consensus reached on them among researchers. This is partly due to the challenges intrinsic to the study of individual membranes. A cellular membrane consists of a bilayer of phospholipids and embedded proteins which is a few nanometers in thickness.[1] The structure puts severe constraints on spectroscopic studies of individual membranes because of its demands on both the sensitivity and the spatial resolution of the measurement. This is particularly critical for the understanding of in-plane nanoscale organization of the lipid and protein components. The latter has been a fundamental issue in membrane biology since the introduction of the fluid mosaic model by Singer and Nicholson[2] and its subsequent development into the lipid raft model by Simons and co-workers.[3]

Over the last few decades, infrared (IR) absorption spectroscopy has been extensively applied to the study of biological systems, thanks to its capability to provide molecular and dynamic information on a broad variety of samples, including single living cells.[4] Many IR spectroscopy studies have been devoted to understanding membranes and their model systems, such as phospholipid bilayers and multibilayers. The available information includes structure and orientation of headgroups, alkyl chains, and embedded proteins, order at the molecular level, phase transitions, lipid−lipid or protein−lipid interactions, and membrane dynamics.[5−7] Most IR absorption measurements have been carried out on samples of macroscopic dimensions, such as vesicle dispersions and multibilayer stacks, using transmission, reflection and attenuated total reflection (ATR) configurations. IR microscopy configurations that rely on far-field optical geometries lack the spatial resolution, because of the limits set by diffraction, and the sensitivity to study nanoscale structure in single bilayers. Because of these constraints, the application of IR microscopy to the study of membranes in vivo has so far been possible only in very specific cases, such as the extended stacks formed by the disks of rod outer segments.[8] The use of a grazing incidence geometry has allowed the selective study of extended bilayers and single leaflets,[9] supported either on solid substrates or at the air−water interface. However, because of the high angle of incidence, these measurements do not provide the spatial resolution necessary to study in-plane membrane organization at the nanoscale. Nanoscale structure

Received: January 29, 2018
Accepted: August 3, 2018
Published: August 3, 2018

DOI: 10.1021/acs.analchem.8b00485
Anal. Chem. 2018, 90, 10179−10186

and reactivity of membranes and bilayers have, to date, escaped direct investigation by IR absorption spectroscopy. Current studies on this scale rely mostly on atomic force microscopy (AFM), to study topographical and mechanical properties, on fluorescence microscopy, for diffusional dynamic studies,[10] or on super-resolved light microscopy,[11] for localization studies.

The introduction of near-field spectroscopic techniques for the IR region has recently provided the sensitivity and spatial resolution to allow the study of soft matter at the nanometer scale.[12] Among these techniques, IR scattering scanning near-field optical microscopy (IR sSNOM or simply sSNOM) and nano-FT-IR[13] have sensitivity and spatial resolution that allow the study of minute amounts of biological material down to the scale of 20 nm.[14] In both techniques, the near-field IR signal from a sample is provided by the localized electric field in the proximity of an externally illuminated, metal coated AFM tip, simultaneously with AFM information.[15] While sSNOM provides images of the sample, nano-FT-IR allows the measurement of extended spectra. Both techniques can be implemented with the same instrument and on the same sample. In the case of sSNOM, an image of the sample is produced by raster scanning under such nanofocused light field at a specific wavelength, thus obtaining the local absorption and reflectivity information. The sSNOM signal is also highly sensitive to crystallinity of the investigated samples such as highly ordered organic materials.[16] In the case of nano-FT-IR, the scattered light from a broadband source is analyzed by Fourier transform of the output of an asymmetric Michelson interferometer while the tip is positioned at a specific location, thus providing the local FT-IR absorption and reflection spectra of the sample.[17] Hyperspectral images of the sample can be obtained by collecting spectra over a 2D array of positions,[18] similarly to other IR near-field techniques.[19]

The capability to provide IR absorption nano-FT-IR spectra and IR sSNOM images of single bilayers of the purple membranes from *H. salinarum* has been demonstrated.[20] However, these studies provided the IR absorption of peptide bonds in patches of bacteriorhodopsin proteins. Measurements on portions of the membrane without bacteriorhodopsin molecules were not reported. The measurement of phospholipid headgroups in a bilayer membrane is expected to be a major challenge, because of their lower concentration within the probed volume compared to the peptide bonds of membrane proteins. A previous attempt to use sSNOM to measure supported phospholipid bilayers relied on the measurement of the ester carbonyl band and provided a limiting sensitivity of three bilayers and an in-plane resolution of about 100 nm.[21]

In this work, we demonstrate the possibility to measure the nanoscale IR absorption of headgroups and alkyl chains in single phospholipid bilayers by using nano-FT-IR and to image their spatial distribution with a resolution better than 40 nm using sSNOM. We use single and multiple bilayers of 1,2-dipalmitoyl-*sn*-glycero-3-phosphocholine (DPPC) on a silicon surface as a model of biological membranes. Despite the compositional simplicity, the system provides a challenge for the sensitivity and spatial resolution of sSNOM and nano-FT-IR that is comparable to the one from real cell membranes.

RESULTS AND DISCUSSION

We deposited single bilayers and multibilayer stacks of DPPC by allowing liposomes to adhere and unfold on the surface of a silicon wafer. The resulting sample, as seen in AFM height maps recorded at room temperature (Figure 1A), displays patches of single and multibilayers separated by areas of exposed silicon surface. Profile analysis shows that each bilayer was about 5.5 nm thick (Figure 1B), as expected for DPPC bilayers below the transition temperature, at 41 °C for a suspension of multilamellar vesicles.[22,23] Multibilayers display a terraced structure that exposes steps corresponding to one, two, three, or more bilayers. In addition, particles can also be observed on top of the bilayers or on the substrate (Figure 1A). Figure S1 compares the AFM height map for a stack of bilayers with the corresponding AFM phase map. The observed difference in phase between the bilayer surface and the surface of the support confirms that the stacks are laying directly on silicon and not on an extended layer of organic material.

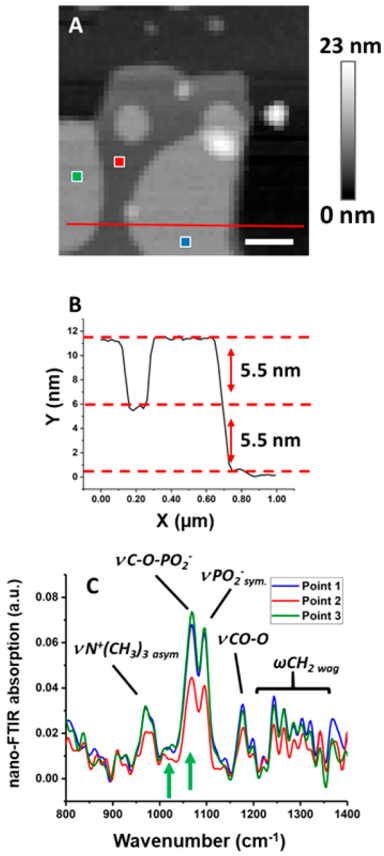

Figure 1. Nano-FT-IR spectroscopic measurements of bilayers of DPPC on a silicon substrate. (A) AFM height image of a region of the sample. The scale bar corresponds to 200 nm. (B) Height profile along the line in panel A. (C) Nano-FT-IR spectra measured at the positions marked in panel A. Spectra are color coded with position markers. Red, single bilayer; blue and green, double bilayers. The nano-FT-IR signal plotted in C is the imaginary part of the measured scattering intensity Im $[\sigma_n(\omega)]$. The green arrows mark the positions that will be used for on-resonance and off-resonance sSNOM imaging in Figure 4.

We use the AFM height map to survey the sample and select positions for the nano-FT-IR spectral measurement, corresponding to different thickness values. Figure 1C shows nano-FT-IR spectra measured with laser power emission in the 800–1400 cm^{-1} range. All quantities used in nano-FT-IR and sSNOM experiments and their relationship are defined in the Supporting Information. In contrast to conventional FT-IR

DOI: 10.1021/acs.analchem.8b00485
Anal. Chem. 2018, 90, 10179–10186

experiments with a glowbar source, which can simultaneously measure the whole mid-infrared spectra region, nano-FT-IR measurements with a DFG source are limited to the measurement of smaller spectral intervals, approximately 600 to 800 cm^{-1} wide, depending on the optical configuration of the source. We selected the 800−1400 cm^{-1} spectral region for our experiments because it allows us to measure simultaneously absorption bands from all functional groups of a phospholipid molecule. The spectra were obtained by plotting the nano-FT-IR absorbance, defined as the imaginary part of the scattering coefficient, $a_n \equiv \mathrm{Im}\,[\sigma_n(\omega)]$ (Supporting Information).[17] The index n is the demodulation order used to extract the scattering signal. The spectra of Figure 1C were obtained from the second harmonic of the modulation frequency. It has been shown that, for weak oscillators, such as in the case of phospholipids, the nano-FT-IR absorbance a_n is proportional to the absorbance as measured in a macroscopic transmission experiment.[17]

Measurements were performed in three different positions, corresponding to single and double bilayers, as marked in Figure 1A. Nano-FT-IR bands are reproduced in all three different locations and in other sample locations (not shown), indicating that they have little contribution from noise. The signal-to-noise ratio for these measurements is in the range 7 to 10 in the central part of the spectral region, where laser intensity is highest, but poorer at the fringes (between 800 and 850 cm^{-1} and 1350−1400 cm^{-1}), where laser intensity tapers off. At the very edge of the spectral range, below 850 cm^{-1} and above 1350 cm^{-1}, decreased reproducibility indicates that noise is overtaking the signal. Comparison of the spectra measured at the three positions in Figure 1A shows that the intensity of the bands from the double bilayer is about 80% to 100% higher than that from the single bilayer. This is expected for bilayers of about 5 nm thickness, which are much thinner than the probing depth of sSNOM, of the order of few tens of nanometers. Figure S2 shows an approach curve on the silicon surface. The curve provides the intensity of the signal (optical amplitude a given Ω_n) as a function of the tip−sample distance. Signal intensity decreases exponentially with tip−sample distance. Therefore, additional bilayers provide an increased contribution to the phase signal as long as they are still within the volume probed by the electric field. Because of the decay of the field away from the tip, the contribution of additional bilayers to the total signal decreases progressively, with little or no increase observed after the fifth bilayer (not shown).

To compare the nano-FT-IR spectra of DPPC in Figure 1 with ATR-FT-IR spectra from macroscopic samples, we deposited a suspension of DPPC liposomes on a diamond ATR prism and allowed it to dry in air. Spectra were recorded soon after the disappearance of the absorption bands from bulk water, to allow the sample to retain some hydration. The resulting spectrum is shown in Figure 2A and compared with one of the nano-FT-IR spectra for a double bilayer. Peak positions were determined using the plot of the second derivative of absorbance (Figure 2B) and are listed in Table 1. Table 1 also lists the band positions of ATR-FT-IR spectra of DPPC reported in the literature.[24]

Band intensity and position in nano-FT-IR spectra are consistent with the spectra of macroscopic samples of DPPC, both from literature data and from our own measurements. The relative intensity and position of most bands in ATR-FT-IR spectra closely match the ones observed in the nano-FT-IR

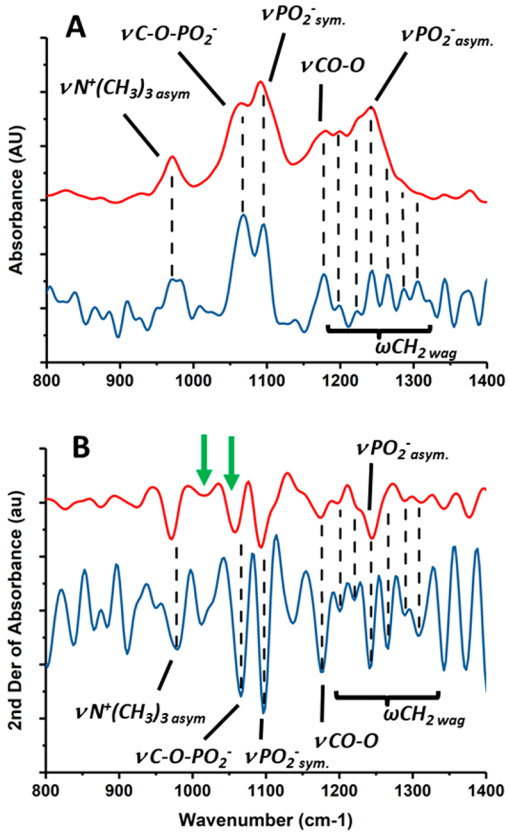

Figure 2. Comparison of nano-FT-IR (blue line) and ATR-FT-IR (red line) spectra of DPPC. (A) ATR-FT-IR spectrum of DPPC and nano-FT-IR spectrum of a double bilayer of DPPC (from Figure 1). The vertical axis plots absorbance units for the ATR-FT-IR spectrum and nano-FT-IR absorbance units for the nano-FT-IR spectrum. The scale is the same for both spectra except that an offset has been applied to the nano-FT-IR spectrum for clarity. (B) Second derivative of the ATR-FT-IR spectrum and of the nano-FT-IR spectrum in panel A. The scale is the same for both spectra except that an offset has been applied to the derivative of the nano-FT-IR spectrum for clarity. The dotted lines show the position of peaks in the nano-FT-IR spectrum and its derivative. The green arrows mark the positions that will be used for on-resonance and off-resonance sSNOM imaging in Figure 4.

spectra. Small differences in band positions reported for the ATR-FT-IR spectra of macroscopic DPPC samples in the literature can be ascribed to both differences in hydration of the samples and differences in the order and packing of bilayers as deposited on the ATR crystal. The only major difference is the relative intensity of the bands at 1198, 1222, and 1243 cm^{-1}. This difference is clearer in the second derivative traces of Figure 2B, confirming that it is due to differences in absorption between the two measurements and not to differences in the baseline. Baseline variations are greatly reduced or canceled by derivation.

Bands in this spectral region are mostly assigned to vibrational modes of phospholipid headgroups, as described in Table 1. In addition, a regular sequence of peaks is observed between 1200 and 1300 cm^{-1} (1200, 1222, 1244, 1265, 1286, 1303, and 1321 cm^{-1}) that corresponds to the progression of the methylene wagging modes of the alkyl chain.[25] Methylene wagging modes have their transition moment aligned along the axis of the extended alkyl chain (Figure 3). The progression arises from the linear combination of wagging modes of individual methylene groups and is observed for highly

DOI: 10.1021/acs.analchem.8b00485
Anal. Chem. 2018, 90, 10179−10186

Table 1. IR Bands of DPPC Bilayers[a]

sSNOM of DPPC	ATR of methyl palmitate	ATR of DPPC[b]	ATR of DPPC[c]	assignment
970		970	970	$\nu N^{+}(CH_3)_{3\ asym}$
1069		1060–1072	1058	$\nu C-O-PO_2^-$
1096		1093	1091	$\nu PO_{2\ sym.}^-$
1178	1177	1178	1180	$\nu CO-O$
1200	1198	1198	1198	$\omega CH_{2\ wag}$
1222	1220	1219	1222	$\omega CH_{2\ wag}$
1244	1242	1242	1243	$\omega CH_{2\ wag}$
*		1255	1243	$\nu PO_{2\ asym.}^-$
1265	1265	1265	1265	$\omega CH_{2\ wag}$
1286	1287	1287	1284	$\omega CH_{2\ wag}$
1303	1310	1310	1314	$\omega CH_{2\ wag}$
1321	1331			$\omega CH_{2\ wag}$

[a]Wavenumbers of bands observed in nano-FT-IR spectra of DPPC in the 800–1400 cm^{-1} spectral region and comparison with values from ATR measurements of oriented methyl palmitate and DPPC and corresponding assignments. The band marked with *, corresponding to the antisymmetric stretching mode ($\nu PO_{2\ asym}^-$), was not observed in nano-FT-IR spectra. [b]Literature data.[24] [c]Values measured in this work.

oriented chains, while it decreases or disappears as the chains become disordered, such as above the gel to liquid transition temperature of phospholipids.[25] In sSNOM and nano-FT-IR measurements, the tip-enhanced electric field is oriented along the axis of the tip and normal to the plane of the bilayer (Figure 3). This geometry allows strong absorption by the wagging modes of the alkyl chains, which extend along the normal to the plane. The regularity of the wagging progression in our nano-FT-IR measurements is comparable to that observed in the ATR spectra of oriented methyl palmitate and DPPC multibilayers.[24] Band position and intensity of the wagging progression indicate that the alkyl chains of the phospholipids are extended and approximately perpendicular to the plane of the bilayer.

One difference from the spectra of macroscopic samples was observed in the intensity of the wagging mode bands at 1198 and 1220 cm^{-1}, which show lower absorption than in ATR-FT-IR spectra. We suggest that this may be due to the thin oxide layer on the Si substrate.[26] The reference measurement was carried out in a region of the substrate without lipids, and Si–O bonds on the surface would add to the reference absorption and provide a negative contribution to the nano-FT-IR spectrum, with the apparent suppression of overlapping bands.

It is notable that in our measurements the absorption of the symmetric stretching mode of the phosphate headgroup ($\nu PO_{2\ sym}^-$) is clearly observed at 1095 cm^{-1}, within 2 cm^{-1} of the value measured by ATR on oriented DPPC films. The absorption of the antisymmetric stretching mode ($\nu PO_{2\ asym}^-$) falls at 1255 cm^{-1} in published ATR-FT-IR spectra[24] and at 1243 cm^{-1} in our own ATR-FT-IR measurements (Figure 2), where its intensity is about half that of $\nu PO_{2\ sym}^-$. In nano-FT-IR spectra (Figure 1), a band is observed at 1244 cm^{-1}. However, it is sharper and weaker than that observed for $\nu PO_{2\ asym}^-$ in ATR-FT-IR spectra of DPPC. Both intensity and bandwidth match those observed in other systems for the $\omega CH_{2\ wag}$ band expected in that position. Therefore, the spectral contribution of $\nu PO_{2\ asym}^-$ is absent or minimal in nano-FT-IR spectra.

The absence of a $\nu PO_{2\ asym}^-$ band can be interpreted considering the orientation of the transition moment for this mode, which has been proposed to lay in the plane of the bilayer.[24] In the DPPC molecule, the transition moment of $\nu PO_{2\ sym}^-$ is aligned along the bisector of the PO_2 group, while the transition moment of $\nu PO_{2\ asym}^-$ is aligned perpendicular to it and in the PO_2 plane.

In the nano-FT-IR experiment, the transition moment is perpendicular to that of the tip-enhanced electric field, making the mode inactive in this experimental geometry (Figure 3). We conclude that the polarization of the $\nu PO_{2\ asym}^-$ transition together with the high degree of orientation of the sample are

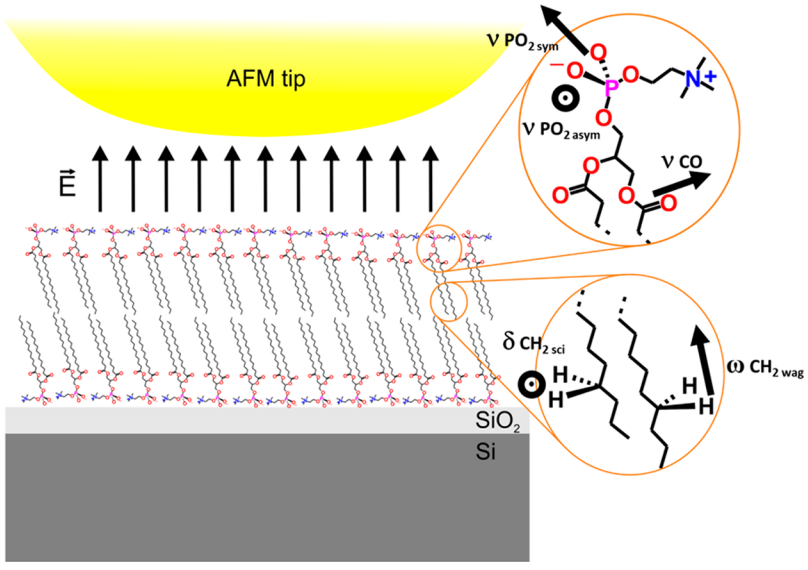

Figure 3. Proposed orientation of DPPC molecules in a bilayer leaflet relative to the incident electric field **E** in the proximity of the tip used for a nano-FT-IR or sSNOM measurement. The figure also shows the orientation of the transition moments (black arrows for vectors in the plane of the page and dotted circles for vectors perpendicular to the plane of the page) for $\nu PO_{2\ sym}^-$, $\nu PO_{2\ asym}^-$, δCH_{2sci}, νCO, and ωCH_{2wag} relative to the DPPC molecule and the field **E**. Dimensions of tip and DPPC molecules are not drawn to scale.

DOI: 10.1021/acs.analchem.8b00485
Anal. Chem. 2018, 90, 10179–10186

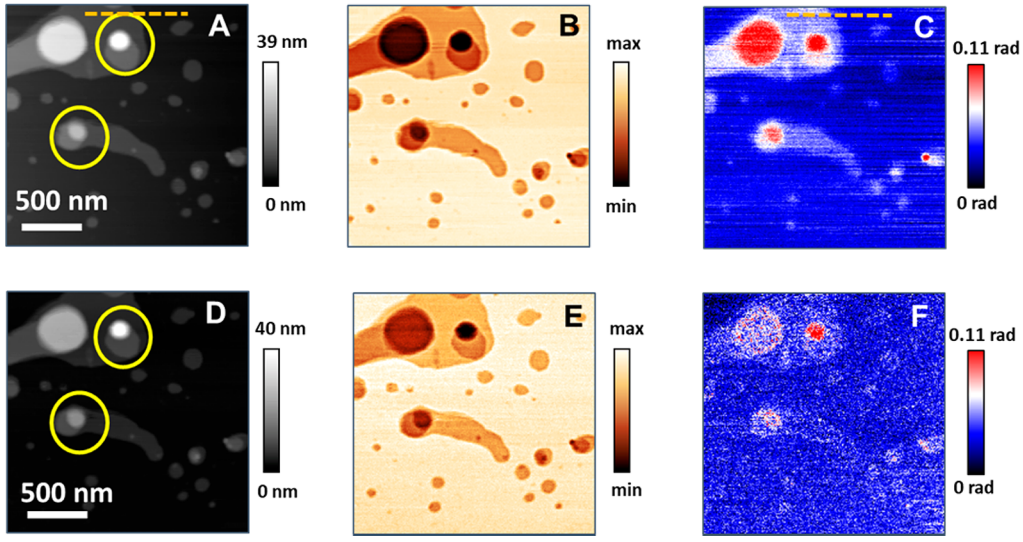

Figure 4. AFM and sSNOM maps of multibilayers of DPPC with single wavelength excitation. (A) AFM topography map recorded while exciting at 1070 cm^{-1} ($\nu C-O-PO_2^-$ band). (B) Reflectivity map at 1070 cm^{-1}, constructed using the amplitude $s(\omega)$ of the scattered light. (C) Absorption map at 1070 cm^{-1}, constructed using the phase $\varphi(\omega)$ of the scattered light. (D) AFM topography map recorded while exciting at 1015 cm^{-1}, where only weak absorption is observed. (E) Reflectivity map at 1015 cm^{-1}. (F) Absorption map at 1015 cm^{-1}. The yellow circles indicate the location of flattened convex particles. The orange dotted lines indicate the positions of line scans used for Figure 5. The wavenumbers used for on-resonance and off-resonance imaging are marked by green arrows in Figure 2B.

the main factors that prevent us from seeing the mode. Therefore, the polarization of the spectra indicates that the PO_2 plane lies approximately perpendicular to the silicon surface.

Madrid and Horswell[27] have shown that, for a bilayer of DPPE in the gel phase supported on an Au (1,1,1) electrode surface, $\nu PO_{2\ asym}^-$ appears as a strong band on top of the wag progression and overlaps with one of the wagging bands, similarly to what we observe in ATR-FT-IR spectra. The intensity of $\nu PO_{2\ asym}^-$ is a function of electrode potential and is stronger for positive potentials, while it disappears for negative potentials. The spectrum at negative potential is very similar to the nano-FT-IR spectrum that we report in Figure 1. The effect has been interpreted as due to increased organization of the headgroups, which align horizontal to the gold surface at negative potential, what is in agreement with our conclusions. This is also consistent with the structure of the oxidized Si surface that supports the phospholipid bilayer in our sample, which is expected to have a negative interfacial charge distribution due to the electron density distribution in the SiO_2 layer.

Figure S3 shows the nano-FT-IR spectrum recorded in the spectral region 1400−1900 cm^{-1}. In FT-IR and ATR FT-IR spectra of macroscopic phospholipid samples, this region is dominated by the two strongest absorption bands, the ester carbonyl stretching mode, νCO, around 1740 cm^{-1}, and the methylene scissoring mode, δCH_{2sci}, around 1470 cm^{-1}. In nano-FT-IR, both appear as weak bands, about 5 to 6 times weaker than phosphate bands. The weakness of these two bands suggests that the transition moments of both δCH_{2sci} and νCO are perpendicular to the electric field of the incident radiation or at a high angle to the normal. The absorption from water around 1640 cm^{-1} is very weak in these spectra, showing that water content is very low. Order and headgroup interactions are known to be favored by a low degree of hydration of the sample, as revealed by changes in thermotropic properties,[28] supporting our conclusions that the sample under investigation is highly ordered.

One possible orientation that satisfies the observed spectral properties is shown in Figure 3. The proposed orientation is expected to be energetically favorable in a bilayer with low hydration because it allows head-to-tail alignment of the electric dipoles of the headgroups. Figure 3 shows the alkyl chains of the two leaflets extended in the parallel structure. However, our data cannot discriminate between this structure and the alternative one with crossed chains, in which the alkyl chains of the two leaflets form the same angle with the normal but with opposite sign.

DPPC for ATR-FT-IR experiments has been prepared by drying vesicle suspensions on the surface of the ATR prism. The resulting samples comprise stacks of bilayers that are fragmented and only partially oriented. In contrast to a nano-FT-IR measurement, an ATR-FT-IR measurement probes the averaged molecular orientation in the whole sample and is unable to appreciate the local order of individual bilayers. Therefore, in ATR-FT-IR measurements, all bands are observed, including $\nu PO_{2\ asym}^-$, even when spectra are collected with perpendicular polarized light.[24] In our ATR-FT-IR measurements, we did not use a polarizer, although some polarization of the beam may still be present because of multiple reflections by instrument optics. Therefore, observation of the $\nu PO_{2\ asym}^-$ band is expected. Furthermore, comparison of nano-FT-IR and ATR-FT-IR spectra shows that bands are sharper in the former, despite the poorer resolution used in nano-FT-IR spectra (10 cm^{-1} versus 8 cm^{-1}). One possible explanation, consistent with other observations in the text, is the higher degree of ordering that can be appreciated when measuring a single nanoscale bilayer, as opposed to a macroscopic stack of bilayers.

The description resulting from the analysis of nano-FT-IR spectra agrees with our current understanding of the structure of phospholipid bilayers and multibilayers below the gel-to-liquid phase transition temperature. Under these conditions

DOI: 10.1021/acs.analchem.8b00485
Anal. Chem. 2018, 90, 10179−10186

multilamellar suspensions of DPPC exist either in the lyotropic liquid crystalline gel phase ($L_{\beta'}$) or in a range of pseudocrystalline phases (L_c).[29] The latter are characterized by in-plane ordering of both the headgroups and the alkyl chains in two-dimensional lattices in supported multibilayers.[30]

Spectra from the single bilayer show small differences in band structure. In particular, the $\nu N^+(CH_3)_{3\ asym}$ band at 970 cm^{-1}, associated with the choline headgroup, shows splitting into two components of equal intensity, at 970 and 982 cm^{-1}, in the single bilayer. In contrast, one of the two components, at 970 cm^{-1}, dominates the spectra of double bilayers. The splitting may be due to the interaction of the lower leaflet with the silicon substrate, which can affect the frequency of the mode. The contribution of this single leaflet can be appreciated in a single bilayer but becomes less obvious when multiple bilayers are present. This is in agreement with recent work by Wu et al.,[31] who reported differences in the properties of individual DPPC leaflets in bilayers supported on mica. The differences were ascribed to the selective interaction of the lower bilayer with the substrate.

We performed IR sSNOM imaging of multibilayer patches by mapping the intensity of the sSNOM signal over the surface of the sample while keeping the emission of the laser fixed at one wavelength. We measured maps at 1070 cm^{-1}, corresponding to the peak of the strong absorption from $\nu C-O-PO_2^-$, and at 1015 cm^{-1}, where only weak absorption can be observed. Figure 4 shows maps of AFM topography, reflectivity, and sSNOM optical phase at the two wavenumbers.

The wavenumber of 1070 cm^{-1} corresponds to the stretching mode of the C−O−P phosphate ester bond, and its spatial distribution tracks that of phospholipid headgroups. Figure 4B shows the reflectivity of the sample at this wavenumber, mapped using the amplitude of the scattered light $s(\omega)$. The reflectivity increases with the real part of the refractive index of the material, $n(\omega)$, giving rise to larger scattering amplitude from reflection at the Si surface ($n(\omega) \sim 3.4$) and lower amplitude from the DPPC bilayers ($n(\omega) \sim 1.5$). Figure 4C maps absorption at 1070 cm^{-1} using the phase $\varphi(\omega)$ of the scattered light. A large contrast is observed due to phospholipid bilayers, which give rise to strong absorption at this wavelength. The phase change increases with the number of stacked bilayers in a given position, as expected from the thickness dependence of the spectra (Figure 1). The same region is mapped while exciting at 1015 cm^{-1}, corresponding to a wavenumber where only weak absorption is displayed by DPPC. At this wavenumber, the reflectivity map still displays weaker but still strong contrast. This is expected since the difference in $n(\omega)$ between silicon and DPPC is still high at this wavenumber. In contrast, weak absorption contrast is observed at 1015 cm^{-1} (Figure 4F) throughout most of the sample and images at this wavenumber show very few structures. A residual phase shift, in the range of 15 mrad, is still observed on the bare Si surface, due to the fact that images retain the phase differences between the maxima but not the absolute phase of the signal. Single bilayers are barely detectable in the 1015 cm^{-1} images, and only thicker sample locations, such as multiple bilayers and round particles, give appreciable contrast.

Figure 5 compares the AFM topography line profile at the edge of a patch with the profile of the phase $\varphi(\omega)$ of the scattered light at 1070 cm^{-1}, showing that the two track closely. The edge profile can be used to provide an estimate for

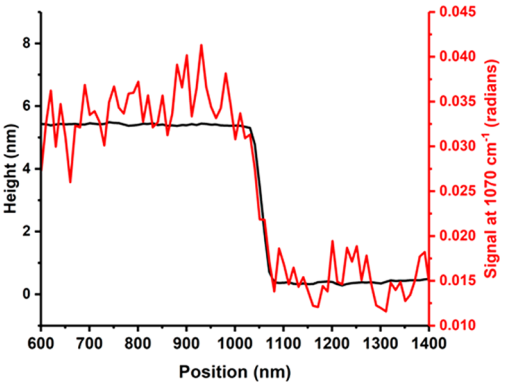

Figure 5. Line profiles across the edge of a bilayer patch, from the images of Figure 4 (Corresponding to the orange dotted lines in Figure 4). Black trace: AFM topography profile. Red trace: profile of the phase of the scattered light $\varphi(\omega)$ at 1070 cm^{-1}.

resolution. To provide statistically significant information, we measured the resolution over 21 edge profiles on the border of one patch. The 90/10 and 80/20 values for resolution (points at 90% and 10% and 80% and 20% of height in the intensity profile) give an average resolution of 51 ± 26 and 39 ± 23 nm, respectively, much smaller than is allowed by diffraction and comparable to the size of the tip (approximately 20 nm diameter). In conclusion, the imaging capabilities of sSNOM of phospholipid bilayers at a selected absorption wavelength are comparable to the ones provided by AFM.

It must be noted that assessing spatial resolution by using a topographical feature, such as an edge, carries the risk that cross-talk between the mechanical and optical measurements may affect the resulting resolution value. In our measurements, any such coupling would be mediated by the tip and would be obvious at the edges of the patches, where the movement of the tip is affected by the change of topography, as evidenced by mechanical phase shifts. For example, the AFM phase map of Figure S1 shows marked edge effects where the phase changes at the edge of each bilayer. However, no edge effects are seen in the map in Figure 4C (the off-resonance map in Figure 4F is too noisy to allow such analysis). The increase of intensity with the number of bilayers observed in Figure 4C also supports the conclusion that image contrast is a function of the amount of material under the tip and not of topography. We conclude that cross-coupling between the mechanical and optical signal is negligible in these measurements and the resolution estimated from Figure 5 is a useful metric for this class of samples.

CONCLUSIONS

We have reported the first detailed IR spectra of a single phospholipid bilayer using a near-field IR technique. We have investigated the spectral region between 800 and 1400 cm^{-1}, which includes bands from both the phospholipid headgroups and their acyl chains. Nano-FT-IR spectra provided the same bands as in the IR absorption spectra of macroscopic samples with similar relative intensities. In addition to band position, the relative intensity of the bands is also fully consistent with their polarization properties and their macroscopic ATR-FT-IR absorption. The observation validates the hypothesis that for a thin film of weak oscillators the nano-FT-IR absorbance, a_n, is proportional to the absorbance measured in a transmission experiment.[17]

DOI: 10.1021/acs.analchem.8b00485
Anal. Chem. 2018, 90, 10179−10186

The average spatial resolution of the measurements is better than 40 nm, consistent with the dimensions of the tip. Overall, the quality of the spectra and the anisotropy displayed by some absorption bands from headgroups and alkyl chains indicate that the DPPC bilayers are highly ordered and oriented. Moreover, the observation of the wagging progression bands indicates that nano-FT-IR measurements can be used to probe nanoscopic changes of order within the bilayers, such as following a phase transition or the interaction with a protein or exogenous molecule. The measurements rely on the intrinsic optical properties of the sample and do not require the introduction of extrinsic chromophores. Therefore, the molecular properties of the system can be studied without any perturbations associated with labeling.

To the best of our knowledge, this is the first time that detailed spectra of single phospholipid bilayers have been obtained by sSNOM and nano-FT-IR. Work by Amenabar et al.[20] provided high-quality spectra of the protein component of single membrane layers. However, the intensity of the signal from membrane phospholipids is about 1 order of magnitude weaker than that from proteins, and it was not observed by these researchers.

The portion of the bilayer probed by the sSNOM experiment corresponds to about 500 nm^2. The footprint of a DPPC molecule in the bilayer plane is approximately 0.5 nm^2. Therefore, the signal for a single bilayer arises from about 2000 (1000 per leaflet) DPPC molecules. Despite the small size of the sample, the quality of the spectra allows detailed molecular studies. It is remarkable that such spatially confined measurements provide such an accurate description of molecular order within a monolayer. The high resolution has to be credited for this advantage, because it allows one to select specific nanosized regions or domains of the sample. In contrast, macroscopic measurements deliver only the average contribution from all regions of the sample. It has already been pointed out that such averaging may be the reason why the polarized ATR-FT-IR spectra of macroscopic samples of phospholipids multibilayers show such variability in literature reports.[8]

It is expected that the studies of the biological membranes for which phospholipid bilayers are models will also be possible in the near future. The major challenge will be, however, the development of sample holders that will allow one to perform sSNOM experiments on samples of biological relevance under controlled environmental conditions, such as bilayers in contact with an aqueous phase or living cells.

METHODS

1,2-Dipalmitoyl-*sn*-glycero-3-phosphocholine (DPPC) was purchased from SIGMA-Aldrich (Poland); chloroform (99%, stabilized with ethanol) was purchased from Avantor Performance Materials (Poland). Deionized water was produced using a Milli-Q deionizer at 18.2 mΩ cm resistivity. Si wafers (P-Type, Boron doped) were purchased from ON Semiconductor (Czech Republic).

A modification of an existing procedure[32] was used for liposome preparation. DPPC was dissolved in chloroform to a concentration of 1 mg/mL and brought to dryness under a flow of gas. The DPPC film was suspended in water to a 1 mg/mL concentration by vortex mixing until a cloudy dispersion was obtained. The dispersion was subjected to five freeze−thaw cycles between liquid nitrogen temperature and 40−50 °C. Finally, the suspension was sonicated in a bath for ∼15 min at a temperature of approximately 45 °C. The liposome suspension was stored at 4 °C.

Supported bilayers and multibilayers were prepared by depositing a drop of the liposome suspension on a Si wafer. The wafers were previously cleaned by immersion for 30 min in piranha solution (50/50 v/v concentrated sulfuric acid and 30% hydrogen peroxide solution in water). *Piranha solution is hazardous and should be handled with extreme care.* Wafers were extensively washed with deionized water and stored under a layer of deionized water. The suspension was allowed to settle for about 1 h and drained by capillary action toward a paper towel touching the side of the wafer.

IR s-SNOM and nano-FT-IR measurements were performed at room temperature with samples exposed to the atmosphere using a neaSNOM system (Neaspec GmbH, Munich) described elsewhere.[17] For nano-FT-IR measurements, a PtIr coated AFM tip (20 nm diameter; 42 N/m force constant) was illuminated using the emission of a coherent, broadband beam from a difference frequency generation (DFG) laser source (Toptica) with 100 fs pulses. The power of the beam was set at 400 μW covering the 700−1500 cm^{-1} (6.7−14 μm) spectral range. The tip was used to probe the sample by operating in tapping mode at the frequency Ω of ca. 250 kHz, thus modulating the intensity of the scattered light at Ω and its higher harmonics. The light backscattered from the tip is analyzed with an asymmetric Michelson interferometer, where the sample and tip are positioned in one arm of the interferometer. A liquid nitrogen-cooled mercury cadmium telluride (MCT) detector was used to measure the intensity of the scattered light. Spectral resolution was set at 10 cm^{-1} with eight levels of zero-filling. Demodulation of the scattered light signal at a higher harmonic $n\Omega$ of Ω was used to separate the contribution of the near-field signal from that of the background and to control the probing depth of the light.[17] Fourier Transform of the interferogram from the beam demodulated at the n-th harmonic $n\Omega$ provides the complex spectra of the scattered electric field $E_n(\omega)$. Near-field spectra of DPPC were normalized by dividing $\langle E_n(\omega)^2\rangle$ by a reference spectrum $\langle E_{n,\mathrm{ref}}(\omega)^2\rangle$ recorded and demodulated at the same $n\Omega$ value on a clean portion of the Si substrate. (See Supporting Information for a definition of the optical quantities.) The normalization corrects for the change in intensity of the laser through the spectral region and between experiments (similarly to what is done when calculating classical IR absorption spectra). The normalization ensures that values of nano-FT-IR absorbance are comparable throughout the spectral region and between the measurements. Noise levels are quantified by dividing two references measured sequentially in the same position of the Si surface. For this purpose, we used the spectral range between 1400 and 2000 cm^{-1}, because of the absence of absorption bands from silicon oxide. Noise levels of 0.007 RMS were measured over the time used to measure the spectra (about 10 min). For the signal intensity value, we used the intensity of the strongest bands in Figure 1, corresponding to 0.05 and 0.07 au for the single and double bilayer, respectively.

sSNOM imaging is performed using a pseudoheterodyne interferometric detection scheme[33] and a tunable QCL laser (Mircat, Daylight Solutions, US) while collecting AFM topography and stiffness information, using the same tip as for nano-FT-IR experiments. The phase $\varphi_n(\omega)$ of the scattered light at the frequency ω_n, demodulated at the n-th order, is mapped as a function of tip position on the sample. Since the

DOI: 10.1021/acs.analchem.8b00485
Anal. Chem. 2018, 90, 10179−10186

phase shift $\varphi_n(\omega)$ is related to absorption (Supporting Information), this provides a map of absorption at the frequency ω superimposed to the topography map. Mapping of the scattered light amplitude $s_n(\omega)$ at the same wavelength provides a map of sample reflectivity at ω.

ATR-FT-IR measurements were performed on a Thermo Nicolet iS10 spectrometer using a Smart iTX diamond ATR accessory, without polarizers. The interferometer was set up for measurements in the mid-IR region using a glowbar source, a liquid nitrogen cooled MCT detector, and a KBr-supported beamsplitter. Measurements were performed at 8 cm^{-1} resolution, and the Fourier Transform was executed with a Blackmann-Harris 3-term apodization function, two levels of zero filling, and a Mertz phase correction algorithm. A suspension of DPPC liposomes, as prepared for sSNOM measurements, was deposited on the diamond ATR crystal and allowed to dry in air. The ATR spectrum was measured soon after the disappearance of absorption bands from bulk water.

Spectral data were analyzed using the program OPUS 7.5 (Bruker Optics) and plotted using the program Origin Pro (Origin Lab, US). AFM and sSNOM images were processed and plotted using the free program Gwyddion 2.50 (http://gwyddion.net/). sSNOM images were corrected for horizontal strokes, row alignment, and row level. All images were corrected to bring the minimum value to zero.

■ ASSOCIATED CONTENT

Supporting Information

The Supporting Information is available free of charge on the ACS Publications website at DOI: 10.1021/acs.analchem.8b00485.

Definition of quantities and relationships; AFM height and phase maps of sample; nano-FT-IR spectrum of 1400−1900 cm^{-1} region; approach curve on silicon (PDF)

■ AUTHOR INFORMATION

Corresponding Author

*E-mail: luca.quaroni@uj.edu.pl.

ORCID

Paweł Wydro: 0000-0002-9145-1362
Mariusz Kepczynski: 0000-0002-7304-6881
Szczepan Zapotoczny: 0000-0001-6662-7621
Maria Nowakowska: 0000-0001-6456-5463
Luca Quaroni: 0000-0002-0225-9775

Notes

The authors declare the following competing financial interest(s): A.C. is an employee of Neaspec GmbH, which produces the instruments for nano-FT-IR and IR sSNOM used in this work.

■ ACKNOWLEDGMENTS

The authors are grateful to Dr. Karol Wolski, Jagiellonian University, for help with FT-IR instrumentation, and to Dr. Magdalena Wytrwał-Sarna, AGH University of Science and Technology, for laboratory access. This project has received funding from the European Union's Horizon 2020 research and innovation program under the Marie Skłodowska-Curie grant agreement No. 665778, managed by the National Science Center Poland under POLONEZ contract UMO-2016/21/P/ST4/01321 (L.Q.)

■ REFERENCES

(1) Nicolson, G. L. *Biochim. Biophys. Acta, Biomembr.* **2014**, *1838* (6), 1451−1466.
(2) Singer, S. J. J.; Nicolson, G. L. L. *Science* **1972**, *175* (4023), 720−731.
(3) Levental, I.; Grzybek, M.; Simons, K. *Proc. Natl. Acad. Sci. U. S. A.* **2011**, *108* (28), 11411−11416.
(4) Quaroni, L.; Zlateva, T. *Analyst* **2011**, *136* (16), 3219.
(5) Dluhy, R. A. *Appl. Spectrosc. Rev.* **2000**, *35* (4), 315−351.
(6) Tamm, L. K.; Tatulian, S. A. *Q. Rev. Biophys.* **1997**, *30* (4), 365−429.
(7) Tatulian, S. A. *Biochemistry* **2003**, *42*, 11898−11907.
(8) Quaroni, L.; Zlateva, T.; Bedolla, D.; Massaro, S.; Torre, V. *ChemPhysChem* **2008**, *9* (10), 1380−1382.
(9) Dluhy, R. A. *J. Phys. Chem.* **1986**, *90* (7), 1373−1379.
(10) Haustein, E.; Schwille, P. *Annu. Rev. Biophys. Biomol. Struct.* **2007**, *36* (1), 151−169.
(11) Kwiatek, J. M.; Hinde, E.; Gaus, K. *Mol. Membr. Biol.* **2014**, *31* (5), 141−151.
(12) Centrone, A. *Annu. Rev. Anal. Chem.* **2015**, *8* (1), 101−126.
(13) Keilmann, F.; Hillenbrand, R. Near-Field Nanoscopy by Elastic Light Scattering from a Tip. In *Nano-Optics and Near-Field Optical Microscopy*; Zayats, A., Richard, D., Eds.; ArtechHouse: Boston, 2009; pp 235−265.
(14) Wiens, R.; Findlay, C. R.; Baldwin, S. G.; Kreplak, L.; Lee, J. M.; Veres, S. P.; Gough, K. M. *Faraday Discuss.* **2016**, *187*, 555−573.
(15) Knoll, B.; Keilmann, F. *Nature* **1999**, *399* (May), 134−137.
(16) Westermeier, C.; Cernescu, A.; Amarie, S.; Liewald, C.; Keilmann, F.; Nickel, B. *Nat. Commun.* **2014**, *5* (May), 4101.
(17) Huth, F.; Govyadinov, A.; Amarie, S.; Nuansing, W.; Keilmann, F.; Hillenbrand, R. *Nano Lett.* **2012**, *12* (8), 3973−3978.
(18) Amenabar, I.; Poly, S.; Goikoetxea, M.; Nuansing, W.; Lasch, P.; Hillenbrand, R. *Nat. Commun.* **2017**, *8*, 14402.
(19) Donaldson, P. M.; Kelley, C. S.; Frogley, M. D.; Filik, J.; Wehbe, K.; Cinque, G. *Opt. Express* **2016**, *24* (3), 1852−1864.
(20) Amenabar, I.; Poly, S.; Nuansing, W.; Hubrich, E. H.; Govyadinov, A. A.; Huth, F.; Krutokhvostov, R.; Zhang, L.; Knez, M.; Heberle, J.; et al. *Nat. Commun.* **2013**, *4*, 2890.
(21) Wollny, G.; Bründermann, E.; Arsov, Z.; Quaroni, L.; Havenith, M. *Opt. Express* **2008**, *16* (10), 7453−7459.
(22) Biltonen, R. L.; Lichtenberg, D. *Chem. Phys. Lipids* **1993**, *64* (1−3), 129−142.
(23) Naumann, C.; Brumm, T.; Bayerl, T. M. *Biophys. J.* **1992**, *63* (5), 1314−1319.
(24) Hubner, W.; Mantsch, H. H. *Biophys. J.* **1991**, *59*, 1261−1272.
(25) Senak, L.; Moore, D.; Mendelsohn, R. *J. Phys. Chem.* **1992**, *96* (15), 2749−2754.
(26) Gokus, T.; Huth, F.; Huber, A. *Microsc. Microanal.* **2015**, *21* (934), 1871−1872.
(27) Madrid, E.; Horswell, S. L. *Langmuir* **2013**, *29* (5), 1695−1708.
(28) Lewis, R.; McElhaney, R. The Mesomorphic Phase Behavior of Lipid Bilayers. In *The Structure of Biological Membranes*, Second ed.; Yeagle, P. L., Ed.; CRC Press: Boca Raton, FL, 2004; pp 53−107.
(29) Lewis, R. N. A. H.; McElhaney, R. N. *Biochim. Biophys. Acta, Biomembr.* **2013**, *1828* (10), 2347−2358.
(30) Raghunathan, V. A.; Katsaras, J. *Phys. Rev. Lett.* **1995**, *74* (22), 4456−4459.
(31) Wu, H.-L.; Tong, Y.; Peng, Q.; Li, N.; Ye, S. *Phys. Chem. Chem. Phys.* **2016**, *18* (3), 1411−1421.
(32) Kepczyński, M.; Nawalany, K.; Jachimska, B.; Romek, M.; Nowakowska, M. *Colloids Surf., B* **2006**, *49* (1), 22−30.
(33) Ocelic, N.; Huber, A.; Hillenbrand, R. *Appl. Phys. Lett.* **2006**, *89* (10), 101124.

DOI: 10.1021/acs.analchem.8b00485
Anal. Chem. 2018, 90, 10179−10186